

The Minimal CFL-Nuclear Interface

Mark Alford^(a), Krishna Rajagopal^(b), Sanjay Reddy^(c), Frank Wilczek^(b)

^(a) Physics and Astronomy Department, Glasgow University, Glasgow, G12 8QQ, U.K.

^(b) Center for Theoretical Physics, Massachusetts Institute of Technology, Cambridge, MA 02139

^(c) Institute for Nuclear Theory, University of Washington, Box 351550, Seattle, WA 98195-1550, USA

May 1, 2001

GUTPA/01/04/03, MIT-CTP-3123, DOE/ER/41132-110-INT01

Abstract

At nuclear matter density, electrically neutral strongly interacting matter in weak equilibrium is made of neutrons, protons and electrons. At sufficiently high density, such matter is made of up, down and strange quarks in the color-flavor locked phase, with no electrons. As a function of increasing density (or, perhaps, increasing depth in a compact star) other phases may intervene between these two phases which are guaranteed to be present. The simplest possibility, however, is a single first order phase transition between CFL and nuclear matter. Such a transition, in space, could take place either through a mixed phase region or at a single sharp interface with electron-free CFL and electron-rich nuclear matter in stable contact. Here we construct a model for such an interface. It is characterized by a region of separated charge, similar to an inversion layer at a metal-insulator boundary. On the CFL side, the charged boundary layer is dominated by a condensate of negative kaons. We then consider the energetics of the mixed phase alternative. We find that the mixed phase will occur only if the nuclear-CFL surface tension is significantly smaller than dimensional analysis would indicate.

1 Introduction

It is becoming widely accepted that at asymptotically high densities, the ground state of QCD with three quark flavors is the color-flavor locked (CFL) phase [1, 2, 3, 4]. In this phase, there is complete spontaneous breaking of the color gauge symmetry, chiral symmetry and baryon number. This phase of QCD is, as we will see below, a transparent, insulating superfluid. Moreover, the effective coupling is weak and the ground state and low-energy properties can be determined by adapting the BCS methods used in the theory of superconductivity [1, 2, 5, 6, 7, 8, 9, 10, 11, 12, 13, 14, 3, 4]. At less-than-asymptotic densities, the CFL phase continues to be the ground state for nonzero quark masses, and even for unequal masses, so long as the differences are not too large [15, 16]. This means that the CFL phase is the ground state for real QCD, in equilibrium with respect to the weak interaction, over a substantial range of densities.

Could the cores of neutron stars, long speculated to contain quark matter, consist of this remarkable phase, whose properties are calculable from first principles? To discover the answer, we must establish observable consequences of the CFL-core hypothesis. A necessary step is to understand the transition(s) between ordinary nuclear matter and CFL quark matter occurring with increasing depth in the neutron star.

The two simplest scenarios are (1) a single sharp interface between nuclear matter and CFL, and (2) a mixed phase region. We construct consistent semi-quantitative models for both. Which is more favorable depends on the surface tension of the interface. We will conclude that for the mixed phase to occur, the surface tension must be significantly less than the value suggested by naive dimensional analysis.

We begin with a brief summary of the general properties of the CFL phase, and overviews of the nuclear-CFL single interface and the mixed phase.

1.1 CFL generalities

The CFL phase consists of equal numbers of u , d and s quarks, and so requires no electrons to make it an electrically neutral, macroscopically allowed bulk phase [17]. The CFL pairing energy, associated with the formation of ud , us , and ds Cooper pairs, is maximized when all three flavors have equal number density. This equality is enforced and the electrical neutrality of the CFL phase is undisturbed even in the presence of a nonzero strange quark mass m_s (up to some critical value).

Although the CFL ground state breaks the color and electromagnetic gauge symmetries, there is an unbroken $U(1)_{\tilde{Q}}$ gauge symmetry and a corresponding massless “rotated” photon given by a specific linear combination of the ordinary photon and one of the gluons [1, 18]. The CFL state is neutral with respect to \tilde{Q} -charge. From now on, whenever we discuss “charge” or “electric field” in the CFL phase we will always be referring to the electrodynamics of the rotated photon that couples to \tilde{Q} .

At temperatures which are small compared to the superconducting gap Δ (of order tens to 100 MeV), the transport and response properties of CFL quark matter are dominated by the lightest excitations. There is an exactly massless superfluid mode, associated with the spontaneous breaking of the exact baryon number symmetry. The lightest charged excitations are the pseudoscalar mesons, which are the pseudo-Nambu-Goldstone bosons associated with spontaneous chiral symmetry breaking [1]. At quark chemical potential μ , these have masses of order $\sqrt{m_s m_{u,d}} \Delta / \mu$, of order ten MeV [6, 7, 8, 9, 11, 12, 13, 14]. The effective field theory which describes these light degrees of freedom is known and at high enough density all coefficients in it can be determined by controlled, weak-coupling calculations [5, 6, 7, 8, 9, 10, 11, 12, 13, 14].

Because there are no electrons, and the charged hadronic modes are gapped, \tilde{Q} -electromagnetic flux, in the form of photons or DC electric or magnetic fields, can penetrate zero-temperature CFL quark matter unimpeded, obeying free Maxwell equations. The zero-temperature CFL phase in bulk is therefore a transparent insulating superfluid, and continues to be so up to temperatures of order tens of MeV, well above the temperature of any neutron star more than a few seconds old.

1.2 Single nuclear-CFL interface

The simplest possibility for a nuclear-CFL interface is that at a single quark chemical potential μ_c , electrically neutral nuclear and CFL matter have equal pressure, and there is a single first order phase transition between the two phases. We will argue below that for nuclear matter, which has a large nonzero electron chemical potential μ_e , to be in stable contact with electron-less CFL matter, a charged boundary layer must develop, extending over both sides of the interface. One aspect of this is a ‘‘QCD-scale’’ micro-boundary region, with a length scale presumably of order one fermi, where the microscopic structures of the different ground states somehow mesh. We will idealize this interface as infinitely thin, and we do not attempt to analyze its details. (In the end, our ignorance of the QCD-scale physics of the micro-boundary will prevent us from giving a completely definitive answer to the question of the stability of the single interface.) Our analysis of the interface focuses on the physics of the charged boundary layers extending over both sides of the micro-boundary. These are tens of fermi wide. They can be analyzed quantitatively based on effective theories for the low-energy degrees of freedom above the bulk ground states on either side of the interface. For the CFL phase, we have such a theory in hand, and we know that it becomes accurate asymptotically. On the nuclear side, there is unfortunately nothing of comparable rigor. We will use a Walecka model, which is well-documented and easy to implement. Eventually, more sophisticated descriptions of the nuclear matter side should be analyzed.

Why is there interesting physics on the ‘macroscopic’ scale, at tens of fermi? Consider attempting to construct a sharp interface, where neutral CFL and nuclear matter meet at a micro-boundary of order 1 fm, on either side of which we find

the respective bulk phases. Due to the difference in chemical potentials, electrons will flow from the nuclear side of the micro-boundary to the CFL side. This flow halts only after an electric field develops, as the residual net positive charge on the nuclear side attracts the electrons on the CFL side, keeping them from penetrating too far into the CFL matter. The outcome is a charge-separated interface, with a layer of positively charged, electron-depleted, nuclear matter on one side and a layer of CFL quark matter with electrons on the other, stabilized by the resulting electric field. The natural length scale for such an electron boundary layer is the electron Debye length, $\lambda_e = \mu_e^{-1} \sqrt{\pi/4\alpha_{\text{em}}} \sim 10$ fm. Note that on the CFL side, the electric field is that associated with $U(1)_{\bar{Q}}$ whereas on the nuclear side, it is that of ordinary electromagnetism.

The electrons are far from being the whole story, however. It turns out that although they set the length scale for the thickness of the charged boundary layers, they do not dominate the charge density. Due to the electric field, protons on the nuclear side pile up near the interface, making this layer even more positive. Similarly, the electric field induces a condensate of negative kaons on the CFL side of the interface, where the kaons are the lightest possible negatively charged excitations. The net negative charge density on the CFL side of the interface is dominated by the kaons, while the positive charge density on the nuclear side is dominated by the protons. We show the electron, proton and kaon number density profiles near a model interface in Fig. 3 in §4.

Due to the separation of charges, the electrostatic potential ϕ is position-dependent. This means that although μ_e is constant across the interface, the “effective” electron chemical potential $\mu_e^{\text{eff}} = (\mu_e + e\phi)$ is position-dependent. Its value is μ_e deep in the nuclear matter and zero deep in the CFL matter. The bulk CFL phase remains electrically neutral even in the presence of a large nonzero μ_e imposed by contact with the nuclear matter because of the presence of a compensating electrostatic potential.

We will calculate the macroscopic density profiles at the minimal interface by using a Thomas-Fermi description for the fermions and a Landau-Ginzburg description for the kaons, and solving a self-consistent equation for the electrostatic potential (essentially, the Poisson equation). The calculation is reminiscent of one previously performed to analyze the electric field at the interface between vacuum and quark matter in the absence of pairing, where electrons spill out of the quark matter [19]. In our case, electrons spill *into* the quark matter from the nuclear matter, and the protons and kaons turn out to play a major role in addition. We present the calculation in §4, after laying the necessary groundwork in §2 and §3. In §2, we describe our models of the bulk CFL and nuclear phases in detail, and in §3, we analyze the interface upon making the simplifying assumption that no kaon condensate occurs on the CFL side.

Let us note several interesting features of the minimal interface.

- The proton and kaon densities are *large*.

- One must take into account the fact that whereas ϕ describes an ordinary electric field on the nuclear side of the interface, it describes a \tilde{Q} field on the CFL side. This means that the electric field ($-\nabla\phi$) must satisfy nontrivial boundary conditions at the interface, dual to those derived for magnetic fields in Ref. [18].
- From the point of view of compact star physics, the most striking feature of the minimal interface is probably the simple fact that it introduces a discontinuity in the density-vs.-radius profile of such a star. For the particular choice of parameters we analyze, nuclear matter with baryon density of $2.1n_0$ and energy density $343 \text{ MeV}/\text{fm}^3$ floats on CFL matter with baryon and energy density both about twice as large, meeting at an interface whose boundary layers are only tens of fermi thick. Here, $n_0 = 0.16 \text{ fm}^{-3}$ is the nuclear saturation density. The consequences of this density discontinuity for the properties of a static compact star and for the dynamics of binary inspiral warrant much further investigation.

1.3 Nuclear-CFL Mixed phase region

As Glendenning realized [20], the bulk energetics does not favor a single interface. Instead, it suggests the existence of a mixed phase region, with domains of positively charged nuclear matter interweaving among domains of negatively charged CFL matter. This phenomenon can be understood from Fig. 1, a schematic phase diagram of QCD in the μ - μ_e^{eff} plane. If one neglects electromagnetism, and thus allows charged bulk phases, nuclear matter is stable in the lighter (yellow) region of Fig. 1 while CFL matter is stable in the darker (violet) region. They meet along a coexistence line, where the two phases have the same chemical potentials and pressure, but different electric charge densities. The CFL phase is electrically neutral on the heavy (red) line given by $\mu_e^{\text{eff}} = 0$. The nuclear phase is electrically neutral along the heavy (red) line through AB .

Two possible paths from nuclear to CFL matter as a function of increasing μ are depicted. In the absence of electromagnetism and surface tension, the favored option is evidently a mixed phase made of negatively charged CFL matter and positively charged nuclear matter along the segment of the coexistence line from A to D . On this segment, positively charged nuclear matter coexists with negatively charged CFL matter, so for pressures in the range P_A to P_D an overall neutral mixed phase can be created by choosing an appropriate volume fraction of CFL relative to nuclear matter. We construct the mixed phase in §6. If, on the other hand, Coulomb and surface energies are large, then the mixed phase is disfavored. The system remains on the nuclear neutrality line up to B , where there is a single interface between nuclear matter at B and CFL matter at C . This minimal interface, which we construct in §4, with its attendant charged boundary layers, occurs between phases with the same μ_e , $\mu = \mu_B = \mu_C$, and pressure P_* . The effective chemical potential

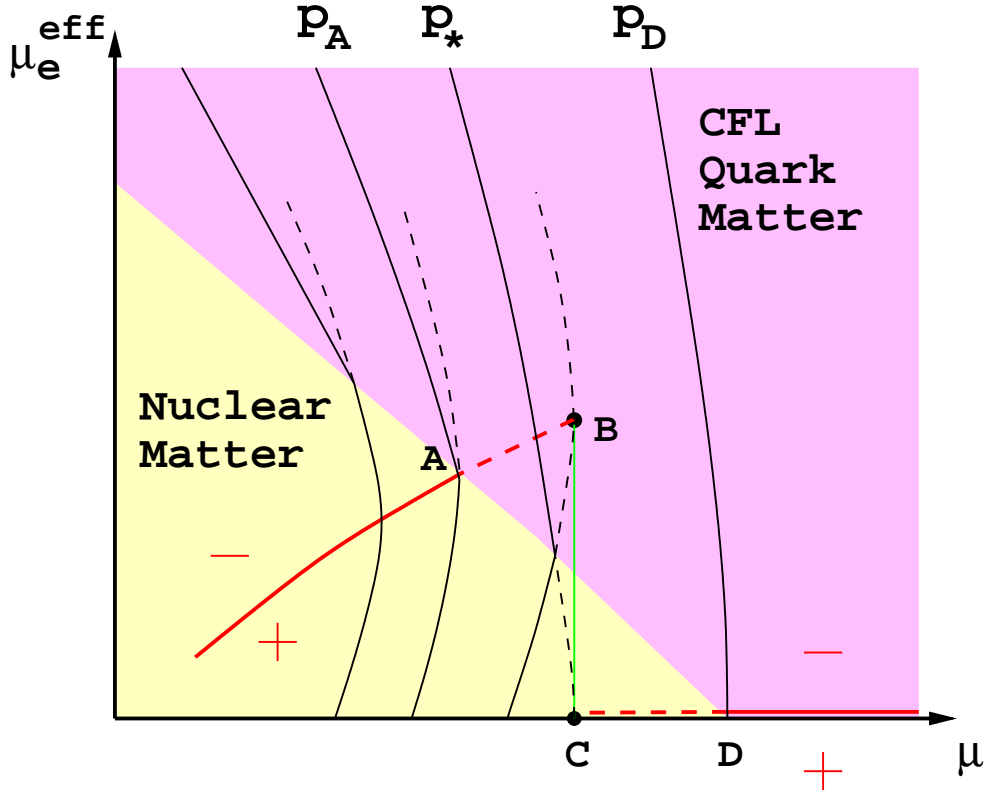


Figure 1: A schematic phase diagram showing the nuclear and CFL phases in the plane of quark chemical potential μ and effective electron chemical potential μ_e^{eff} . Isobars are shown as thin solid lines, and neutrality lines for nuclear and CFL matter are thick (red) lines. Each phase is negatively charged above its neutrality line, and positively charged below it. Continuation onto the unfavored sheet is shown by broken lines.

μ_e^{eff} changes across the interface, though, as a result of the presence of the electric field.

So, is the minimal interface as previously described stable? To decide between the single interface and mixed phase scenarios, we must consider the cost of making multiple interfaces, that is the surface tension.

The surface tension of the single interface turns out to be dominated by the cost of the macroscopic boundary layer, rather than the “fundamental” surface tension σ_{QCD} of the micro-boundary. We calculate the boundary layer surface tension in §5, and find that it is quite large: about $420 \text{ MeV}/\text{fm}^2$. This result alone does not preclude the existence of a mixed phase, however. Rather, it constrains the size of the domains in such a mixed phase to be small compared to the 10 fm length scale characteristic of the boundary layers that dress a single interface. If the mixed

phase has small enough Wigner-Seitz cells, density profiles do not vary much within a single cell, and the surface energy reverts to σ_{QCD} . In §6 we show that while a mixed phase region is guaranteed to occur for small enough σ_{QCD} , the single interface constructed in §4 is more stable than the mixed phase if $\sigma_{\text{QCD}} \gtrsim 40 \text{ MeV}/\text{fm}^2$. On the other hand, naive dimensional analysis suggests $\sigma_{\text{QCD}} \sim 300 \text{ MeV}/\text{fm}^2$.

1.4 Other possibilities

Throughout the remainder of the paper, we will adopt the minimal hypothesis that nuclear matter composed of neutrons, protons and electrons, known to exist at densities of order n_0 , and CFL matter, known to exist at asymptotically large densities, exhaust the content of a neutron star. We conclude this introduction, however, by mentioning some of the many *non*-minimal possibilities.

If the transition from nuclear to quark matter occurs at too large a density, then interesting complications may arise on the nuclear side; if it occurs at too small a density, interesting complications may arise on the quark side.

If the transition to quark matter occurs at a high enough density, it will be preceded by the onset of kaon condensation [21] and/or by the onset of nonzero hyperon density. Either kaon condensation or the presence of hyperons will tend to reduce μ_e . If the hyperon number densities get sufficiently large that hyperon-nucleon pairing occurs, it may even be possible for the transition to the CFL phase to occur continuously [22, 15]! (Note that the transition from ordinary nuclear matter to the CFL phase cannot be continuous, since it involves a change in symmetry.)

If the transition to quark matter occurs at a low density or equivalently, since the relevant parameter is $m_s^2/(4\mu\Delta)$, if the effective strange quark mass at the transition is too large or the gap is too small, then the transition may occur to a less symmetric form of quark matter, in which CFL pairing does not occur. Ordinary BCS pairing may still occur between quarks of two out of three flavors. There will certainly be electrons present in order to maintain neutrality. The quarks which cannot undergo BCS pairing may well undergo LOFF pairing [23], making the matter a crystalline color superconductor [24, 25, 26]. In this non-minimal scenario, it is only as the density increases further that a subsequent phase transition to quark matter in the CFL phase occurs.

2 Bulk Neutral CFL vs. Bulk Neutral Nuclear Matter

In this section, we construct the free energies of electrically neutral nuclear and CFL matter, choose parameters, and find the chemical potential at which the two phases have equal pressure. These provide the basis for analyzing the density profile of model neutron stars containing a CFL quark core and a single interface. We leave that analysis, and an analysis of how the location of the interface varies as parameters are changed, to future work. Here, for concreteness, we settle on one reasonable set of parameters.

2.1 The CFL phase...

We describe the CFL phase using the free energy [3, 17]

$$\Omega_{\text{CFL}} = \frac{6}{\pi^2} \int_0^\nu p^2(p - \mu)dp + \frac{3}{\pi^2} \int_0^\nu p^2 \left(\sqrt{p^2 + m_s^2} - \mu \right) dp - \frac{3\Delta^2\mu^2}{\pi^2} + B, \quad (2.1)$$

where the quark number densities are $n_u = n_d = n_s = (\nu^3 + 2\Delta^2\mu)/\pi^2$ and the common Fermi momentum is

$$\nu = 2\mu - \sqrt{\mu^2 + \frac{m_s^2}{3}} \approx \mu - \frac{m_s^2}{6\mu}. \quad (2.2)$$

Let us discuss each term in turn. The first two terms give the free energy of the u and d quarks, assumed massless, and s quarks with their mass m_s , in the absence of interactions. However, the number densities are *not* what they would be in the absence of interactions. CFL pairing forces all flavors to have the same Fermi momentum and hence the same number density, as long as m_s is not too large [17]. The next term is the leading contribution (in powers of Δ/μ) of the CFL pairing to the free energy [3], and is valid¹ whether the interaction which causes the pairing is treated as some phenomenological four-quark interaction or as the exchange of a propagating gluon [3]. (The calculation of Δ is quite different in these two cases, but the contribution to the free energy is as in (2.1) as long as Δ/μ is small.) The derivation of the first three terms in Ω_{CFL} is given in Ref. [17], which uses a simplified two-quark model, but the generalization to the nine quarks of the CFL phase is straightforward. The final term is a bag constant, which we use as a simple phenomenological way of parametrizing the physics of confinement.

It would certainly be possible to include additional physical effects to what appears in Ω_{CFL} . For example, we are neglecting the perturbative interactions among the quarks [27]. The CFL pairing, which we do include, has qualitative effects which play a crucial role in the following. Including the perturbative effects would simply have the effect of increasing Ω_{CFL} at a given μ . The fact that we leave this out means that to obtain a reasonable phenomenology, we must choose larger values of B than are typically used when the perturbative effects are included [28].

It is worth noting that in the CFL phase the value of μ corresponding to a given pressure $P = -\Omega$ depends sensitively on P and on the bag constant B , but only weakly on the gap Δ and on m_s , as long as both are small compared to $(B + P)^{1/4}$. This can be seen by rewriting (2.1) as

$$\frac{1}{2}\mu^2 = \sqrt{\frac{1}{3}\pi^2(B + P)} + \frac{1}{4}m_s^2 - \Delta^2 + \dots \quad (2.3)$$

¹The numerical coefficient in front of this term is quantitatively valid if the CFL condensate is purely in the color- $\bar{\mathbf{3}}$, flavor- $\mathbf{3}$ channel. There must, in fact, be a small additional condensate in the color- and flavor-symmetric channel [1, 3, 4], but this makes a negligible contribution to the free energy.

to lowest order in Δ and m_s .

The electromagnetic properties of CFL matter will be crucial in subsequent sections, so we review them here. In QCD with three flavors, electromagnetism is described by a $U(1)_{\text{EM}}$ symmetry which is a gauged subgroup of the flavor group $SU(3)_L \times SU(3)_R$. In the CFL phase, each separate $SU(3)$ in the $SU(3)_{\text{color}} \times SU(3)_L \times SU(3)_R$ symmetry of the Lagrangian is spontaneously broken, but the symmetry $SU(3)_{\text{color}+L+R}$ associated with simultaneous color and flavor rotations remains unbroken. One $U(1)$ subgroup of this unbroken $SU(3)_{\text{color}+L+R}$ symmetry is a linear combination of $U(1)_{\text{EM}}$ and a $U(1)$ subgroup of the original color symmetry. Once we are alerted to this possibility, it is not difficult to identify the appropriate combination of the photon and one gluon which remains unbroken [1, 18]. It is generated by

$$\tilde{Q} = Q + \eta T_8 \quad (2.4)$$

where Q is the conventional electromagnetic charge generator, T_8 is associated with one of the gluons, and in the representation of the quarks,

$$\begin{aligned} Q &= \text{diag}\left(\frac{2}{3}, -\frac{1}{3}, -\frac{1}{3}\right) \text{ in flavor } u, d, s \text{ space,} \\ \eta T_8 &= \text{diag}\left(-\frac{2}{3}, \frac{1}{3}, \frac{1}{3}\right) \text{ in color } r, g, b \text{ space.} \end{aligned} \quad (2.5)$$

By construction, the \tilde{Q} -charges of all the Cooper pairs in the CFL condensate are zero. (For example, with these conventions red up quarks pair only with green down or blue strange quarks, and both these pairs have $\tilde{Q} = 0$ in sum.) The condensate is \tilde{Q} -neutral, the $U(1)$ symmetry generated by \tilde{Q} is unbroken, the associated \tilde{Q} -photon will remain massless, and within the CFL phase the \tilde{Q} -electric and \tilde{Q} -magnetic fields satisfy Maxwell's equations. The linear combination of the photon and the eighth gluon which remains massless is

$$A_\mu^{\tilde{Q}} = \frac{gA_\mu + \eta e G_\mu^8}{\sqrt{\eta^2 e^2 + g^2}} = \cos \alpha_0 A_\mu + \sin \alpha_0 G_\mu^8 \quad (2.6)$$

with $\eta = 1/\sqrt{3}$, while the orthogonal combination

$$A_\mu^X = \frac{-\eta e A_\mu + g G_\mu^8}{\sqrt{\eta^2 e^2 + g^2}} = -\sin \alpha_0 A_\mu + \cos \alpha_0 G_\mu^8, \quad (2.7)$$

gets a mass and the corresponding X -magnetic field experiences a Meissner effect. The denominators arise from keeping the gauge field kinetic terms correctly normalized, and we have defined the angle α_0 which specifies the unbroken $U(1)$ via

$$\cos \alpha_0 = \frac{g}{\sqrt{\eta^2 e^2 + g^2}}. \quad (2.8)$$

The mixing angle α_0 is the analogue of the Weinberg angle in electroweak theory, in which the presence of the Higgs condensate causes the A_μ^Y and the third $SU(2)_W$

gauge boson to mix to form the photon, A_μ , and the massive Z boson. At accessible densities the gluons are strongly coupled ($g^2/(4\pi) \sim 1$), and of course the photons are weakly coupled ($e^2/(4\pi) \approx 1/137$), so $\alpha_0 \simeq \eta e/g$ is small, perhaps of order $1/20$. The rotated photon consists mostly of the usual photon, with only a small admixture of the T_8 gluon.

All the elementary excitations in the CFL phase (the pseudo-Goldstone bosons, the massive vector bosons, the gapped fermions) couple to $A_\mu^{\tilde{Q}}$ with charges which are integer multiples of

$$\tilde{e} = \frac{eg}{\sqrt{\eta^2 e^2 + g^2}} = e \cos \alpha_0, \quad (2.9)$$

the \tilde{Q} -charge of the electron, which is less than e because the electron couples only to the A_μ component of $A_\mu^{\tilde{Q}}$. The only massless excitation, the superfluid mode corresponding to spontaneous violation of baryon number, is \tilde{Q} -neutral. Because all charged excitations have nonzero mass, and there are no electrons present, the bulk CFL phase at low temperatures is a transparent insulator.

In the vicinity of the interface with nuclear matter, electrons (with charge $-\tilde{e}$), the negative kaons (same charge) and the \tilde{Q} -electric field will all play a role.

Before attempting a comparison between Ω_{CFL} and Ω_{nuclear} , we must determine for what values of Δ , m_s and μ the CFL phase is more stable than less symmetric quark matter, i.e. quark matter in the absence of CFL pairing, rendered electrically neutral by the presence of a nonzero electron density. In the CFL phase, even though μ_e takes on the same value as that in the nuclear matter with which it is in contact, the effective electron chemical potential $\mu_e + \tilde{e}\phi = 0$ and the electron density vanishes. In unpaired quark matter, weak equilibrium imposes $\mu_u = \mu - \frac{2}{3}\mu_e$ and $\mu_d = \mu_s = \mu + \frac{1}{3}\mu_e$ and electrical neutrality turns out to require

$$\mu_e = \frac{m_s^2}{4\mu} - \frac{m_s^4}{48\mu^3} + \dots \quad (2.10)$$

where the higher order terms are suppressed by further powers of m_s^2/μ^2 . We can therefore evaluate the difference between the free energy of neutral CFL quark matter and neutral unpaired quark matter. We find:

$$\Omega_{\text{CFL}} - \Omega_{\text{unpaired}} = -\frac{3}{\pi^2}\Delta^2\mu^2 + \frac{3}{16\pi^2}m_s^4, \quad (2.11)$$

to lowest nonzero order in Δ/μ and m_s^2/μ^2 . This means that as long as

$$\Delta > \frac{m_s^2}{4\mu} \quad (2.12)$$

the free energy gained from CFL pairing is greater than the free energy cost of maintaining equal quark number densities. This criterion for the stability of the

CFL phase relative to that of neutral unpaired quark matter is the analogue of that derived in Ref. [17] in a simplified two-quark model, although the numerical coefficient in (2.12) differs from that in the model of Ref. [17].

Actually, the decisive comparison is not that between CFL pairing and no pairing at all. Rather one should compare the free energy of the CFL phase with that of some “2SC phase” wherein standard BCS pairing occurs between either up and down quarks only or up and strange quarks only. The quarks which do not participate in the 2SC condensate may form a crystalline color superconducting phase [24, 25, 26], in which quarks with differing Fermi momenta pair with each other, or else quarks of the same flavor may pair among themselves to form spin-1 condensates [29]. Either form of secondary pairing, single-flavor or crystalline color superconducting, make only negligibly small corrections to the free energy. Inclusion of the 2SC condensate affects the competition between CFL quark matter and less symmetrically paired quark matter mainly by reducing the coefficient in (2.12) from 1/4 to a somewhat smaller value, no less than $1/\sqrt{12}$. Since this has little impact on the present paper, and the analysis includes features of independent interest, we will defer it to a subsequent publication.

2.2 The nuclear matter phase . . .

We could make many of the qualitative points we wish to make if we idealized the nuclear matter side of the interface as noninteracting neutrons, protons and electrons. However, if we want to work with estimates of the numerical values of the number densities near the interface which are potentially illustrative, we must incorporate the strong interactions among the neutrons and protons in some way. In this initial effort, we choose to use a Walecka-type relativistic field theoretical model in which the nucleons interact with omega, rho and sigma mesons [30]. The nuclear-CFL interface could and should be studied using less simplified treatments of the nuclear matter side. The Lagrangian we use for the nucleon sector is given by

$$\begin{aligned} \mathcal{L}_N = & \bar{\Psi}_N \left(i\gamma^\mu \partial_\mu - m_N^* - g_{\omega N} \gamma^\mu V_\mu - g_{\rho N} \gamma^\mu \vec{\tau}_N \cdot \vec{R}_\mu \right) \Psi_N \\ & + \frac{1}{2} \partial_\mu \sigma \partial^\mu \sigma - \frac{1}{2} m_\sigma^2 \sigma^2 - U(\sigma) - \frac{1}{4} V_{\mu\nu} V^{\mu\nu} \\ & + \frac{1}{2} m_\omega^2 V_\mu V^\mu - \frac{1}{4} \vec{R}_{\mu\nu} \cdot \vec{R}^{\mu\nu} + \frac{1}{2} m_\rho^2 \vec{R}_\mu \cdot \vec{R}^\mu, \end{aligned} \quad (2.13)$$

where $m_N^* = m_N - g_{\sigma N} \sigma$ is the nucleon effective mass, which is reduced compared to the free nucleon mass m_N due to the scalar field σ , taken to have $m_\sigma = 600$ MeV. The vector fields corresponding to the omega and rho mesons are given by $V_{\mu\nu} = \partial_\mu V_\nu - \partial_\nu V_\mu$, and $\vec{R}_{\mu\nu} = \partial_\mu \vec{R}_\nu - \partial_\nu \vec{R}_\mu$ respectively. The scalar self-interaction term is given by

$$U(\sigma) = \frac{b}{3} m_N (g_{\sigma N} \sigma)^3 + \frac{c}{4} (g_{\sigma N} \sigma)^4, \quad (2.14)$$

where b and c are dimensionless coupling constants. Ψ_N is the nucleon field operator with $\vec{\tau}_N$ the nucleon isospin operator. The five coupling constants, $g_{\sigma N}$, $g_{\omega N}$, $g_{\rho N}$, b , and c , are chosen as in Ref. [31] to reproduce five empirical properties of nuclear matter at saturation density: the saturation density itself is $n_0 = 0.16 \text{ fm}^{-3}$; the binding energy per nucleon is 16 MeV; the nuclear compression modulus is 240 MeV; the nucleon effective mass at saturation density is $0.78m_N$; and the symmetry energy is 32.5 MeV.

The model is solved in the mean-field approximation, wherein only the time component of the meson fields have nonzero expectation values. The symbols σ , ω and ρ denote sigma, omega and rho meson expectation values that minimize the free energy given by [30]

$$\begin{aligned} \Omega_{\text{nuclear}}(\mu_n, \mu_e) = & \frac{1}{\pi^2} \left(\int_0^{k_{Fn}} dk k^2 (\varepsilon_n(k) - \mu_n) + \int_0^{k_{Fp}} dk k^2 (\varepsilon_p(k) - \mu_p) \right) \\ & + \frac{1}{2} (m_\sigma^2 \sigma^2 - m_\omega^2 \omega^2 - m_\rho^2 \rho^2) + U(\sigma) - \frac{\mu_e^4}{12\pi^2}, \end{aligned} \quad (2.15)$$

where

$$\varepsilon_n(k) = \sqrt{k^2 + m_N^{*2}} + g_{\omega N} \omega - \frac{1}{2} g_{\rho N} \rho, \quad (2.16)$$

$$\varepsilon_p(k) = \sqrt{k^2 + m_N^{*2}} + g_{\omega N} \omega + \frac{1}{2} g_{\rho N} \rho, \quad (2.17)$$

are the neutron and proton single particle energies in the mean field approximation. The corresponding Fermi momenta k_{Fn} and k_{Fp} , which minimize the free energy at fixed baryon and electron chemical potentials, are given by solving

$$\begin{aligned} \varepsilon_n(k_{Fn}) &= \mu_n, \\ \varepsilon_p(k_{Fp}) &= \mu_p, \end{aligned} \quad (2.18)$$

where weak equilibrium sets $\mu_p = \mu_n - \mu_e$, and

$$\begin{aligned} m_\sigma^2 \sigma &= g_{\sigma N} (n_s(k_{Fn}) + n_s(k_{Fp})) - \frac{dU}{d\sigma}, \\ m_\omega^2 \omega &= g_{\omega N} (n(k_{Fn}) + n(k_{Fp})), \\ m_\rho^2 \rho &= \frac{1}{2} g_\rho (n(k_{Fp}) - n(k_{Fn})). \end{aligned} \quad (2.19)$$

The nucleon number density n and scalar density n_s for nucleons with Fermi momentum k_F are

$$\begin{aligned} n(k_F) &= \frac{1}{\pi^2} \int_0^{k_F} dk k^2 = \frac{k_F^3}{3\pi^2}, \\ n_s(k_F) &= \frac{1}{\pi^2} \int_0^{k_F} dk k^2 \frac{m_N^*}{\sqrt{k^2 + m_N^{*2}}}. \end{aligned} \quad (2.20)$$

Note that in Eq. (2.15), the electron contribution has also been included. In bulk matter, the condition $\partial\Omega_{\text{nuclear}}/\partial\mu_e = 0$, which enforces electric charge neutrality, uniquely determines μ_e . The magnitude and the density dependence of the electron chemical potential is sensitive to the value of the nuclear symmetry energy, parametrized in this model as the strength of the isovector interaction.

2.3 ... and their meeting point

The critical quark chemical potential, μ_c , above which the electrically neutral CFL state has lower free energy than nuclear matter is determined by requiring $\Omega_{\text{CFL}}(\mu_c) = \Omega_{\text{nuclear}}(\mu_n = 3\mu_c, \mu_e)$. (In Fig. 1, $\mu_c = \mu_B = \mu_C$.) Both μ_c and the critical pressure $P_c = -\Omega_{\text{CFL}}(\mu_c)$ depend sensitively on the high density behavior of the nuclear EOS and on the numerical value of the bag constant. They are less sensitive to the value of the gap, as Eq. (2.3) suggests. For the nuclear equation of state described in the previous section, and for CFL-phase parameters given by: $B^{1/4} = 190$ MeV, $m_s = 150$ MeV and $\Delta = 100$ MeV, we find that $\mu_c = 365$ MeV. The corresponding electron chemical potential on the nuclear side, required to ensure electrically neutral bulk nuclear matter, is $\mu_e = 214$ MeV. The pressure at the interface is 34 MeV/fm³. The baryon density on the nuclear side is $n_B^{\text{nuclear}} = 2.1 n_0$ and on the CFL side is $n_B^{\text{CFL}} \simeq 4.3 n_0$. In estimating $n_B^{\text{CFL}} = -\partial\Omega_{\text{CFL}}/\partial\mu$, we have treated Δ as μ -independent.² The energy density on the nuclear side is 343 MeV/fm³ and on the CFL side is 719 MeV/fm³. Note that with the parameters just described, the criterion (2.12) is satisfied by a factor of more than six in the quark matter at μ_c . This justifies our assumption that the quark matter is in the CFL phase. It is only if Δ were significantly smaller or if the effective strange quark mass m_s were significantly larger that we would find a transition from nuclear matter to a less symmetric form of quark matter (with 2SC and crystalline color superconducting condensates) followed at a larger μ by a second transition to the CFL phase.

As an illustration of the sensitivity to B , if we reduce $B^{1/4}$ to 171 MeV, CFL matter with density $2.7 n_0$ becomes stable at *zero* pressure. To give a sense of the effects of CFL-pairing on these bulk properties, note that if we had not included the effects of CFL-pairing in Ω_{CFL} , we would have found that unpaired strange quark matter was stable at zero pressure only for $B^{1/4} = 155$ MeV, instead of 171 MeV. Looked at another way, with a fixed choice of $B^{1/4}$ (for example 190 MeV as we use), CFL pairing lowers the free energy of the CFL phase, thus increasing its pressure, and therefore reduces the values of P_c and μ_c at which the interface with nuclear matter occurs, relative to previous estimates made using unpaired quark matter. Although a more systematic study incorporating effects like the perturbative interaction among quarks would be necessary before making contact with various phenomenological normalizations of B [28], we expect this qualitative

²With the parameters we have chosen, the $\Delta^2\mu^2$ term of (2.1) only contributes at the level of $\Delta^2/\mu^2 \sim 10\%$ to the number density, so any reasonable μ -dependence of Δ will contribute below this level.

feature to be robust. As a consequence, CFL-quark matter will extend closer to the surface of a compact star than previously estimated for unpaired quark matter.

Leaving construction of neutron star models and the systematic exploration of the dependence of the location of the interface on parameters like B , m_s and Δ for future work, we turn now to the physics occurring at the CFL-nuclear interface, wherever it occurs.

3 The Minimal Interface Without Kaons

The bulk calculation of the previous section gives us μ and μ_e at the nuclear-CFL interface. We now set up the calculation of the number densities near the interface. We choose a geometry where a sharp phase boundary exists at $z = 0$, the region $z < 0$ contains nuclear matter and the region $z > 0$ contains CFL quark matter. As previously explained, the physics of concern here occurs on the 10 fm distance scale, so we do not attempt to resolve the internal structure of the micro-boundary, instead encapsulating its properties in boundary conditions at $z = 0$. The region near the interface is characterized by a positive charge density on the nuclear side and a negative \tilde{Q} -charge density on the CFL side. As a result, there is an electric field $\vec{E}(z)$ on the nuclear side and a \tilde{Q} -electric field $\vec{E}_{\tilde{Q}}(z)$ on the CFL side, which we express in terms of an electrostatic potential ϕ ,

$$\begin{aligned}\vec{E}(z) &= -\vec{\nabla}\phi & z < 0 & \text{ (nuclear) ,} \\ \vec{E}_{\tilde{Q}}(z) &= -\vec{\nabla}\phi & z > 0 & \text{ (CFL) .}\end{aligned}\tag{3.1}$$

The boundary condition for perpendicular electric field at the interface is simply

$$\begin{aligned}\vec{E}_{\tilde{Q}}(0^+) &= \cos \alpha_0 \vec{E}(0^-) , \\ \text{i.e. } \partial_z \phi(0^+) &= \cos \alpha_0 \partial_z \phi(0^-) ,\end{aligned}\tag{3.2}$$

which is dual to the condition derived for perpendicular magnetic fields in Ref. [18]. The underlying physics is that the electric field entering the CFL phase from the nuclear phase is resolved into a \tilde{Q} component, which penetrates into the CFL region, and an orthogonal X -component which is screened out. The CFL condensate carries X -charge, and screens X -flux on a length scale of order $1/\Delta$, which is short compared the electron Debye length λ_e . This justifies our treating it by a boundary condition. In reality, we see from (2.8) that $\cos \alpha_0$ is very close to unity³ so in most of our calculations we set $\cos \alpha_0 = 1$. In Fig. 5 we illustrate the effects of α_0 on the interface using the exaggerated case $\cos \alpha_0 = 1/2$.

The boundary conditions at infinity, deep in the nuclear and CFL phases, are

$$\begin{aligned}\partial_z \phi(-\infty) &= 0 & \text{ (nuclear) ,} \\ \partial_z \phi(+\infty) &= 0 & \text{ (CFL) .}\end{aligned}\tag{3.3}$$

³ As the \tilde{Q} dielectric constant in the CFL phase is slightly different from one [32], the ratio in (3.2) is slightly smaller than $\cos \alpha_0$, but is still very close to unity.

These follow from the fact that the star as a whole is neutral, as are the bulk CFL and nuclear phases.

The electron chemical potential μ_e must be constant across the interface, otherwise electrons would flow. However, the electron density is controlled by the effective electron chemical potential

$$\begin{aligned}\mu_e^{\text{eff}}(z) &= \mu_e + e\phi(z) & z < 0, \\ &= \mu_e + \tilde{e}\phi(z) & z > 0,\end{aligned}\tag{3.4}$$

which is z -dependent, enabling the electron density to vary across the interface. The fact that the CFL phase is neutral in the absence of electrons means that $\mu_e^{\text{eff}}(+\infty) = 0$, allowing the boundary conditions to be expressed as

$$\begin{aligned}\phi(-\infty) &= 0 & \text{(nuclear)}, \\ \phi(+\infty) &= -\mu_e/\tilde{e} & \text{(CFL)}.\end{aligned}\tag{3.5}$$

To obtain the density profiles we solve the Poisson equation

$$\frac{d^2\phi}{dz^2} = e\rho_Q(z),\tag{3.6}$$

subject to the boundary conditions above, where ρ_Q is the electric charge density. On the CFL side of the interface, e is replaced by \tilde{e} . We solve Poisson's equation in the local density or Thomas-Fermi approximation, where the charge density is written in terms of position-dependent Fermi momenta $k_{Fp}(z)$ and $k_{Fe}(z)$ for protons and electrons respectively:

$$\rho_Q(z) = \frac{k_{Fp}^3(z) - k_{Fe}^3(z)}{3\pi^2}.\tag{3.7}$$

(In this section we neglect the light charged bosons in the CFL phase, which give a further contribution to the charge density which cannot be described via a local Fermi momentum; these effects will be included in the next section.) The Thomas-Fermi approximation is valid if ϕ , and hence k_{Fp} and k_{Fe} , vary only on length scales which are long compared to $1/k_{Fe}$ and $1/k_{Fp}$. That is, we require $dk_{Fe,p}/dz \ll k_{Fe,p}^2$. We have checked that the profiles we find satisfy this condition at the 5% level. This confirms our expectation that the local Fermi momenta vary on a length scale of order $\lambda_e \sim 10$ fm. In addition to justifying our use of the Thomas-Fermi approximation, this justifies our treating the 1 fm scale physics via boundary conditions at $z = 0$.

For non-interacting electrons and protons, the local Fermi momenta can be simply expressed in terms of the z -independent chemical potentials μ_e and μ_n and the electrostatic potential $\phi(z)$

$$\begin{aligned}k_{Fe}(z) &= \mu_e^{\text{eff}}(z) \\ k_{Fp}^2(z) &= (\mu_p - \mu_e^{\text{eff}}(z))^2 - m_N^2\end{aligned}\tag{3.8}$$

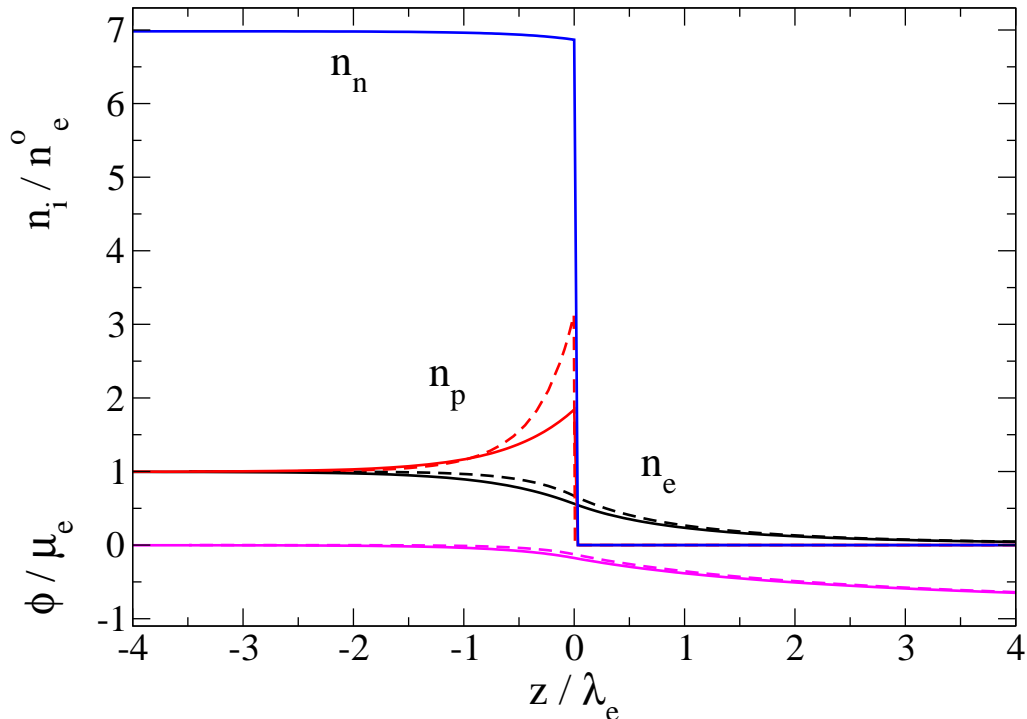


Figure 2: Particle number density profiles and electrostatic potential ϕ near a sharp interface between nuclear matter and CFL quark matter. Distance is measured in units of the electron Debye length $\lambda_e = \mu_e^{-1} \sqrt{\pi/4\alpha_{\text{em}}} \sim 10$ fm. In constructing these boundary layers, we have neglected the possibility of a kaon condensate on the CFL side. The transition occurs at $\mu = \mu_n/3 = 365$ MeV and an electron chemical potential $\mu_e = 214$ MeV. Solid curves show results which include effects due to strong interactions between baryons. Dashed curves show results where they are neglected.

where $\mu_p = \mu_n - \mu_e = \sqrt{\mu_n^2 + m_N^2}$ is the proton chemical potential. It is fixed by requiring electrical neutrality deep in the nuclear matter region: $k_{Fp}(-\infty) = k_{Fe}(-\infty)$. To include the effects of strong interactions among the nucleons, instead of using the equation above for k_{Fp} one must solve the equations of the Walecka model given in §2, which yield k_{Fp} and k_{Fn} as a function of μ_n and μ_e^{eff} (Eqs. (2.18) and (2.19)).

The Thomas-Fermi equation for ϕ is an ordinary second-order differential equation, which we have numerically solved using both shooting methods and relaxation methods. Our results for the electrostatic potential ϕ and the resulting particle density profiles are given in Fig. 2. The distance z from the interface is given in units of the electron Debye screening length $\lambda_e = \mu_e^{-1} \sqrt{\pi/4\alpha_{\text{em}}}$. The dashed curves are the density profiles assuming nuclear matter made of noninteracting neutrons, protons and electrons. The solid curves show the effects of including the strong interactions among the nucleons using the Walecka model described in §2.

Notice that because protons and neutrons are strongly coupled, the neutron density readjusts slightly near the interface to ensure constant baryon chemical potential.

Because the electrons are taken to be massless, the electrostatic potential and the electron density in the CFL phase exhibit power law falloff $k_{Fe} = \mu_e^{\text{eff}} \sim 1/z$.

4 The Minimal Interface With Kaons

Because the CFL condensate breaks chiral symmetry, the lightest charged degrees of freedom in this phase are the resulting Nambu-Goldstone excitations. These are light but not massless once nonzero quark masses are taken into account. The pseudoscalar bosons can be analyzed in terms of an effective field theory with the Lagrangian [5, 6]

$$\mathcal{L}_{\text{eff}} = \frac{f_\pi^2}{4} \text{Tr} (\partial_0 \Sigma \partial_0 \Sigma^\dagger + v_\pi^2 \partial_i \Sigma \partial^i \Sigma^\dagger) + c (\det M \text{Tr}(M^{-1} \Sigma) + \text{h.c.}) , \quad (4.1)$$

where we have retained only terms with two derivatives. The color singlet $\Sigma = \exp i\sqrt{2}\mathcal{B}/f_\pi$ transforms under $SU(3)_L \times SU(3)_R$ and describes the octet of pseudoscalar mesons defined by the 3×3 matrix \mathcal{B} . The masses of the pseudoscalar mesons associated with chiral symmetry breaking can be obtained from the structure of the mass terms in the above Lagrangian [6, 11]. The pion and kaon masses are given by

$$m_{\pi^\pm}^2 = \frac{2c}{f_\pi^2} m_s (m_u + m_d) , \quad m_{K^\pm}^2 = \frac{2c}{f_\pi^2} m_d (m_u + m_s) . \quad (4.2)$$

Thus, the kaon is lighter than the pion, by a factor of $m_d/(m_u + m_d)$ [6]. We have neglected instanton effects which induce a small $\langle \bar{q}q \rangle$ condensate in the presence of a CFL condensate. The resulting additional contribution to the meson masses [1, 8], is likely small [33, 3].

At asymptotically high densities, the full theory is weakly coupled and the coefficient c appearing in the mass term, the velocity of the modes v_π and the decay constant f_π can therefore all be calculated from first principles. Up to possible logarithmic corrections, they are given by [6, 7, 8, 9, 11, 12, 13, 14, 3]

$$f_\pi^2 = \frac{21 - 8 \log 2}{36\pi^2} \mu^2 , \quad v_\pi^2 = \frac{1}{3} , \quad c = \frac{3\Delta^2}{2\pi^2} . \quad (4.3)$$

At the densities of interest to us, these asymptotic expressions can certainly not be trusted quantitatively, although we shall use them in order to be concrete.

As first noted in the CFL context by Schäfer [33], a nonzero electron chemical potential may drive the condensation of negatively charged Goldstone bosons. This renders the matter negatively charged, and therefore cannot occur in bulk CFL matter. The bulk CFL phase has $\mu_e^{\text{eff}} = 0$. We find that meson condensation does occur within the negatively charged boundary layer on the CFL side of the interface.

At first encounter, one might expect that negative kaons (which have charge $-\tilde{e}$ like the electrons) condense if $\mu_e^{\text{eff}} > m_K$ and negative pions condense if $\mu_e^{\text{eff}} > m_\pi$. This is not the case, however. Even if $\mu_e^{\text{eff}} > m_\pi$, it is always more favorable to make (lighter) kaons than pions. Simply put, pions can always decay into kaons. We have confirmed by explicit calculation that if we incorporate the possibility of both pion and kaon condensation, only kaon condensation occurs. For simplicity of presentation, therefore, we retain only the kaon fields in the meson matrix \mathcal{B} .⁴ We characterize the kaon condensate by an amplitude θ and rewrite charged kaon fields as

$$\mathcal{B} = \begin{pmatrix} 0 & 0 & K^+ \\ 0 & 0 & 0 \\ K^- & 0 & 0 \end{pmatrix} \quad \text{with} \quad K^\pm = \frac{f_\pi \theta}{\sqrt{2}} \exp(\mp i \mu_e^{\text{eff}} t). \quad (4.4)$$

Substituting this into Eq. (4.1), we find that free energy density associated with the K^- condensate is given by

$$\Omega_K(\mu, \mu_e^{\text{eff}}) = -\frac{f_\pi^2}{2} \left((\mu_e^{\text{eff}})^2 \sin^2 \theta + v_\pi^2 (\vec{\nabla} \theta)^2 + 4m_K^2 \sin^2(\frac{1}{2}\theta) \right). \quad (4.5)$$

Varying Ω_K with respect to ϕ (which enters in Ω_K via μ_e^{eff}) yields a new contribution to the right hand side of the Poisson equation. Varying Ω_K with respect to θ yields a new differential equation because of the $\vec{\nabla} \theta$ term. It turns out, however, that wherever the kaon density is appreciable, this spatial gradient term in Ω_K is negligible. More precisely, for the 80% of kaons closest to the interface, the $\vec{\nabla} \theta$ term is always 5% or less of the kaon free energy. We therefore drop the spatial gradient term, and solve explicitly for the condensate amplitude by minimizing Ω_K , obtaining $\theta(z)$ from $\cos \theta(z) = m_K^2 / (\mu_e^{\text{eff}}(z))^2$. Thus, we can rewrite the free energy in the following compact form:

$$\Omega_K(\mu, \mu_e^{\text{eff}}) = -\frac{1}{2} f_\pi^2 \mu_e^{\text{eff}2} \left(1 - 2 \frac{m_K^2}{(\mu_e^{\text{eff}})^2} + \frac{m_K^4}{(\mu_e^{\text{eff}})^4} \right). \quad (4.6)$$

The kaon number density is then

$$n_K(\mu, \mu_e^{\text{eff}}) = \frac{\partial \Omega_K(\mu, \mu_e^{\text{eff}})}{\partial \mu_e} = f_\pi^2 \mu_e^{\text{eff}} \left(1 - \frac{m_K^4}{(\mu_e^{\text{eff}})^4} \right). \quad (4.7)$$

All these expressions are only valid for $\mu_e^{\text{eff}} > m_K$; for smaller μ_e^{eff} , there is no kaon condensate: $\theta = n_K = 0$.

When $m_K \ll \mu_e$ the Debye screening length of kaons is given by $\lambda_K = (\sqrt{4\pi\alpha_{em}} f_\pi)^{-1} \lesssim 10$ fm. We therefore expect that kaons are as (or even more) effective than electrons at screening the electric field in the CFL boundary layer,

⁴If higher order corrections to the effective field theory for the Nambu-Goldstone bosons in the CFL phase were to make the π^- lighter than the K^- , we would of course obtain pion condensation rather than kaon condensation.

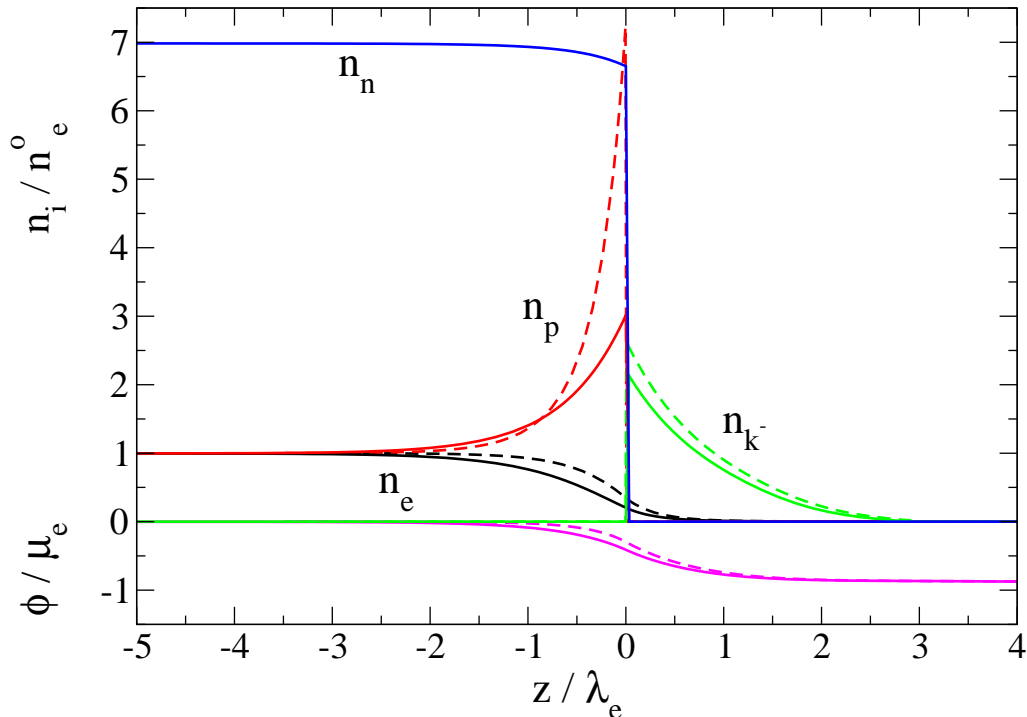


Figure 3: Particle number density profiles and electrostatic potential ϕ near a sharp interface between nuclear matter and CFL quark matter, including the possibility of kaon condensation on the CFL side. As in Fig. 2, the transition occurs at $\mu = \mu_n/3 = 365$ MeV and an electron chemical potential $\mu_e = 214$ MeV. Solid curves show results which include effects due to strong interactions between baryons. Dashed curves show results where they are neglected.

and should be included in a realistic description of the interface. This is easily done by including their contribution to the electric charge density in the source term of Poisson's equation. Particle profiles obtained upon including kaons in the CFL phase are shown Fig. 3. We see that the negative charge density in the CFL boundary layer is dominated by kaons, which are much more numerous than the electrons. This can be understood upon noting that wherever $\mu_e^{\text{eff}} > m_K$, the kaon density would rise without bound if the kaons were noninteracting bosons. It is only their Coulomb repulsion and the interactions encoded in the nonlinear effective Lagrangian for the kaons that stabilize their number density. Since electrons are fermions, their density is controlled by μ_e^{eff} even in the absence of interactions. The figure also shows that the increased negative charge on the CFL side of the interface, due to the kaons, increases the electric field on the nuclear side of the interface, thus resulting in an even larger pileup of protons than we found in §3. Note that we have neglected higher derivative terms in the kaon effective field theory (4.1). This is justified wherever $\mu_e^{\text{eff}}/\Delta$ is small. The analysis of higher order terms in Ref. [10] suggests that they can be neglected for $\mu_e^{\text{eff}} < (1 - 1.5)\Delta$. To see that this condition

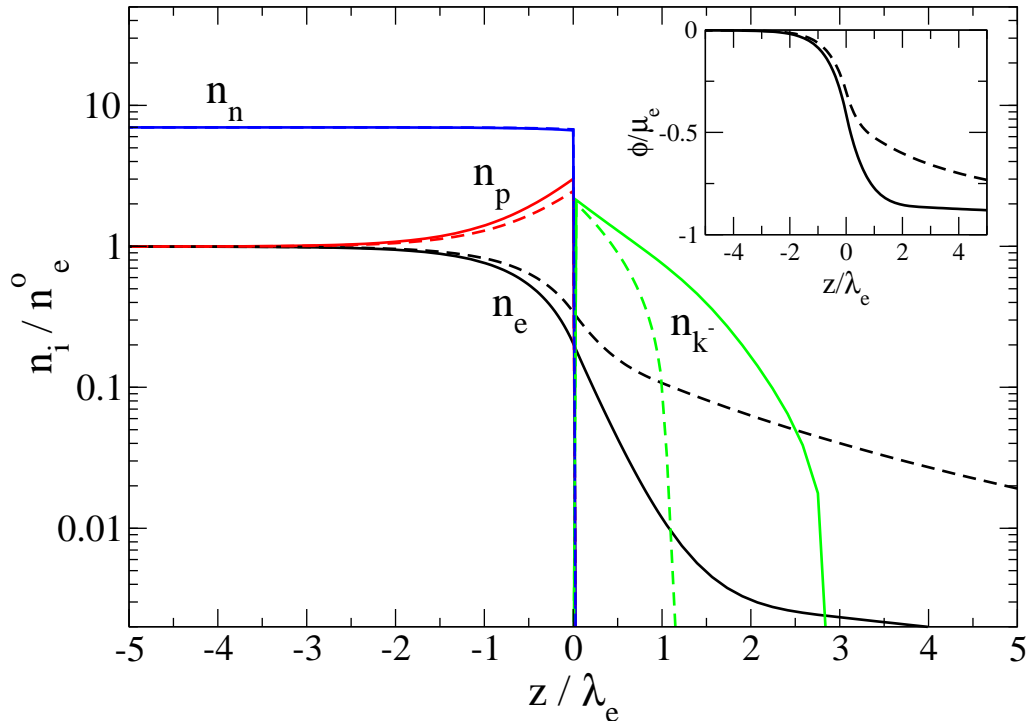


Figure 4: As in Fig. 3, but with number densities shown on a logarithmic scale and with the electrostatic potential shown as an inset. The solid curves are for $m_K = 28$ MeV, as obtained from (4.2) and as in Fig. 3. The dashed curves are for $m_K = 100$ MeV. The strong interactions among the nucleons are included.

is satisfied for the profiles shown in Fig. 3, note that because of the presence of the protons on the nuclear side of the interface, μ_e^{eff} is at most $\sim \mu_e/2$ on the CFL side.

We see from Fig. 4 that if the kaon mass is greater than that obtained from (4.2), which is after all only quantitatively valid at asymptotically large densities, the maximum kaon density is somewhat reduced. More significantly, since kaon condensation occurs only where $\mu_e^{\text{eff}} > m_K$, the kaon condensate does not extend as deep into the CFL phase for larger values of m_K . Because we continue to take the electrons to be massless, we find that, as in Fig. 2, the electron density in the CFL phase has a power law tail, with $k_{Fe} \sim 1/z$ at large z . For $m_K = 28$ MeV, the amplitude of this power law tail is greatly reduced, however, because most of the screening on the CFL side is now done by the kaon condensate. For larger values of m_K , there is less charge in the kaon condensate because its depth is reduced, and the amplitude of the power law tail of the electron density consequently increases, as the profiles become more similar to those of Fig. 2.

In Fig. 5, we show the profiles at an interface in a theory in which the mixing angle which relates the ordinary photon to the \tilde{Q} -photon of the CFL phase is not small: we take $\cos \alpha_0 = 0.5$. We see, for example, that the electron density is discontinuous because electrons have charge e on the nuclear side of the interface

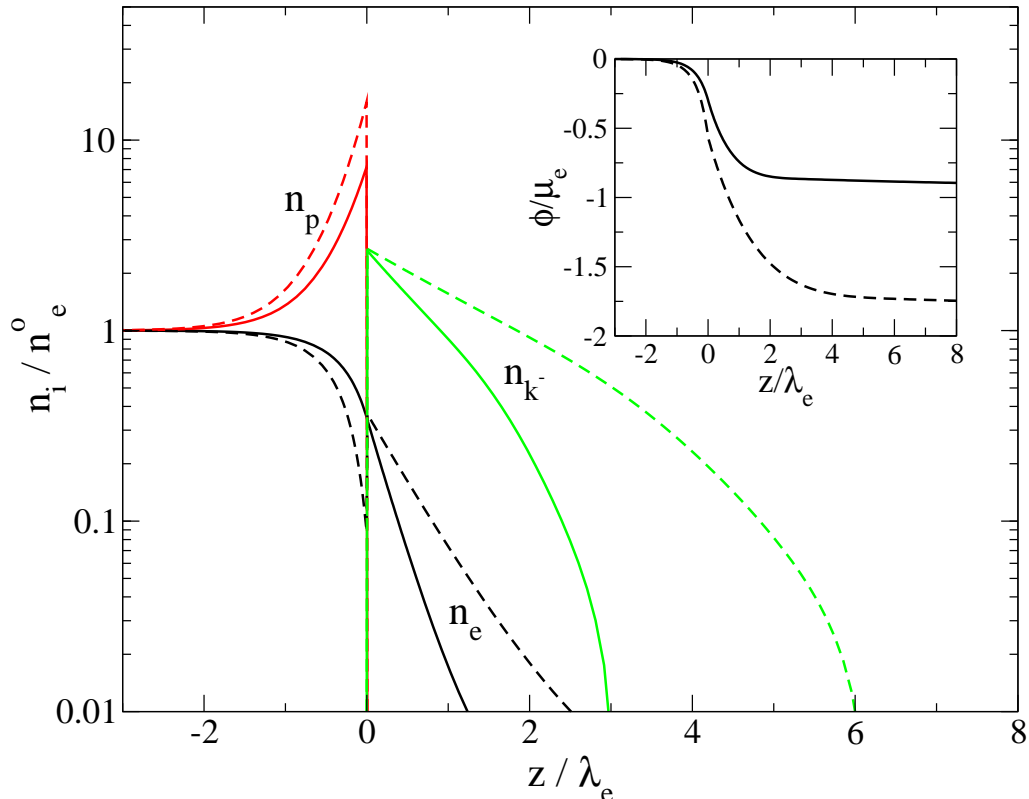


Figure 5: As in Fig. 3, but for two values of the mixing angle α_0 . The solid curves are for $\cos \alpha_0 = 1$, as in all other figures. The dashed curves are for $\cos \alpha_0 = 0.5$. The strong interactions between nucleons have been turned off. This figure illustrates the consequences of the fact that $\tilde{e} < e$ and $\vec{E}_{\tilde{Q}} > \vec{E}$ by dramatically exaggerating them.

and charge $\tilde{e} = e \cos \alpha_0$ on the CFL side. In nature $\alpha_0 \sim 1/20$, so taking $\cos \alpha_0 = 1$ as we do in all other figures is certainly adequate.

5 Surface Tension

Having determined the profiles which characterize the minimal interface between CFL and nuclear matter, we now wish to investigate the stability of this sharp interface. We have already seen in Fig. 1 that if we neglect surface tension, the sharp interface must be less stable than a broad mixed phase region, denoted in that figure by the line AD . Before constructing this mixed phase, therefore, let us see what we can learn about the surface tension of the single sharp interface.

There are two contributions to the surface tension. The first is that due to the QCD-scale interface which we treat as sharp. We have no quantitative calculation of this surface tension, which we denote σ_{QCD} , but we can estimate it by dimensional

analysis. The difference between the energy densities at $z = 0^+$ and $z = 0^-$ in, for example, the interface described by the solid curves in Fig. 3 is about $325 \text{ MeV}/\text{fm}^3$. If we estimate that the transition from CFL to nuclear matter occurs over a distance of about 1 fm, we expect

$$\sigma_{\text{QCD}} \sim 300 \text{ MeV}/\text{fm}^2 \quad (5.1)$$

This estimate is based only on dimensional analysis and could easily be a significant overestimate.

The second contribution to the surface tension of the single interface is that due to the boundary layers whose profiles we have constructed. Again, we focus on the profiles shown as solid curves in Fig. 3. We must integrate the difference between the z -dependent energy density described by these number densities and the energy density of the undisturbed bulk CFL or nuclear phase. Solving the Poisson equation ensures that the pressure throughout the boundary layers is constant, and thus equal to that of the bulk phases. This means that the interface has no extra free energy. The energy density difference is therefore determined by the difference between the “ μN ” terms for the z -dependent profile and the undisturbed bulk phases. Hence, the contribution of the boundary layers to the surface tension is

$$\begin{aligned} \sigma_{\text{boundary layer}} = & \int_{-\infty}^0 dz \left(\mu_n [n_n(z) - n_n(-\infty)] \right. \\ & + [\mu_n - \mu_e^{\text{eff}}(z)] n_p(z) - [\mu_n - \mu_e] n_p(-\infty) \\ & \left. + \mu_e^{\text{eff}}(z) n_e(z) - \mu_e n_e(-\infty) \right) \\ & + \int_0^{\infty} dz \left(\mu_e^{\text{eff}}(z) n_e(z) + \mu_e^{\text{eff}}(z) n_K(z) \right), \end{aligned} \quad (5.2)$$

where $n_{e,K}(z)$ are the electron and kaon number densities in the CFL boundary layer and $n_{n,p,e}(z)$ are the neutron, proton and electron number densities in the nuclear boundary layer. We find

$$\sigma_{\text{boundary layer}} \simeq 420 \text{ MeV}/\text{fm}^2 \quad (5.3)$$

for the profiles in Fig. 3. Because μ_n and μ_p are much larger than μ_e , and because n_n deviates little from its bulk value, the boundary layer contribution to the surface tension is in fact dominated by the contribution of the protons. We see that as a result of the development of charged boundary layers, and in particular as a result of the pileup of protons, the surface tension of the minimal CFL-nuclear interface is large and the dominant contribution is calculable.

6 Mixed Phase

If we neglect the surface tension and the Coulomb interaction then, as discussed in the introduction, the minimal CFL-nuclear interface is not stable because a broad

mixed phase region has lower free energy. The observation that a mixed phase may exist is neither new nor specific to the nuclear-CFL transition. In earlier work, Glendenning showed that because of the existence of two independent chemical potentials, corresponding to conserved electric charge and baryon number, a mixed phase is a generic possibility wherever a first order phase transition occurs within a neutron star [20]. Subsequently, the first order transition between nuclear matter and unpaired quark matter was investigated by several authors [20, 34, 35]. In these studies, wherein surface and Coulomb effects were either chosen to be small or neglected, a mixed phase was shown to be favored over a wide range of pressure.

We begin this section with an explicit construction of the Glendenning-style mixed phase in the present context, neglecting the effects of surface tension and the Coulomb interaction. We shall restore these effects below. Phase coexistence is possible if the Gibbs condition of equal pressures and equal baryon chemical potentials is satisfied. (To maintain consistency of notation, we work with the quark chemical potential μ ; that for baryon number is 3μ .) At fixed μ , we find the electron chemical potential which satisfies the pressure equality condition

$$P_{\text{CFL+kaons}}(\mu, \mu_e) = P_{\text{nuclear}}(\mu, \mu_e) , \quad (6.1)$$

where $P_{\text{CFL+kaons}}$ describes the pressure of the negatively charged phase obtained by imposing $\mu_e > 0$ on the CFL phase, thus creating a condensate of negatively charged kaons. This phase would have infinite (actually, nonextensive) free energy in bulk, due to the Coulomb repulsion. When it occurs in a mixed phase, the Coulomb energy cost (evaluated below) is finite. Note that no significant electric fields develop in the mixed phase, meaning that $\mu_e^{\text{eff}} = \mu_e$ therein. As $\mu_e \neq 0$ is uncompensated by any electrostatic potential, wherever $\mu_e > m_e$ we expect electrons and wherever $\mu_e > m_K$ we expect a condensate of negatively charged kaons.

The condition (6.1) uniquely determines the pressure and μ_e as a function of the baryon chemical potential at which phase coexistence is possible. Clearly, the μ_e obtained as a solution to Eq. (6.1) does not correspond to the μ_e required to ensure the electrical neutrality of either phase. Electric charge neutrality is therefore enforced only as a global condition. This condition determines the volume fraction χ of the CFL+kaon phase via

$$\chi Q_{\text{CFL+kaons}} + (1 - \chi) Q_{\text{nuclear}} = 0 , \quad (6.2)$$

where Q_{nuclear} is the charge density of the nuclear phase, $Q_{\text{CFL+kaons}}$ that of the CFL phase with kaons.

In Fig. 6 we present the results of such a calculation. Several quantities that characterize: i) the neutral nuclear phase; ii) the nuclear-CFL mixed phase; and iii) the neutral CFL phase are shown. The electron chemical potential in the charge neutral nuclear phase is shown in solid black. It increases with increasing baryon chemical potential to compensate for electric charge density of the protons. The pressure of the electrically neutral nuclear matter phase is also shown. At

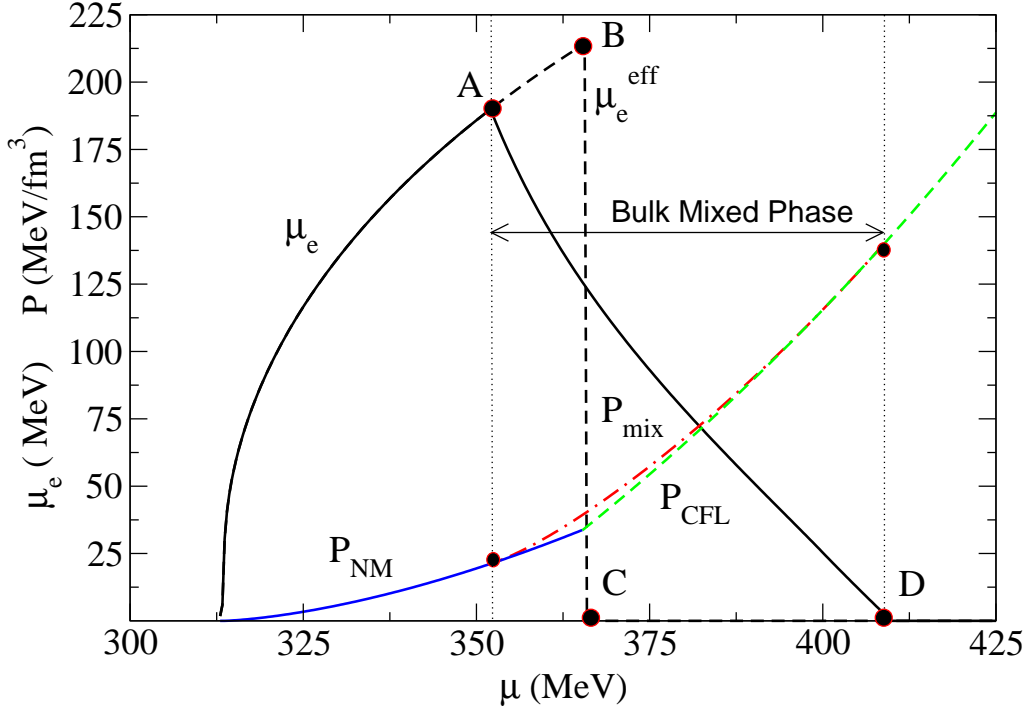


Figure 6: Behavior of the electron chemical potential and the pressure of homogeneous neutral nuclear and CFL matter and of the mixed phase, all as a function of the quark chemical potential μ . Only bulk free energy is included; surface and Coulomb energy is neglected. As in Fig. 1, the mixed phase occurs between A and D . The vertical line connecting B and C denotes the μ at which the pressures of neutral CFL and nuclear matter are equal. This is where a sharp interface may occur. The pressure of the mixed phase exceeds that of neutral CFL or neutral nuclear matter between A and D . Were this the whole story, the mixed phase would evidently be favored over the sharp interface.

$\mu = 352$ MeV, at the point A , the pressure of the electrically neutral nuclear matter phase and the negatively charged CFL+kaon phase coincide. Above this density, it becomes energetically favorable to construct a electrically neutral mixed phase wherein a positively charged nuclear phase coexists with a negatively charged CFL+kaon phase. At A , the negatively charged CFL phase containing kaons is constructed with the same value of μ_e as that in the charge neutral nuclear phase. For larger values of μ , the pressure and electron chemical potential of both the nuclear and CFL phases is obtained by solving Eq. (6.1). The pressure in the mixed phase is shown as the dot-dashed curve. In the mixed phase, μ_e decreases with increasing μ . The mixed phase ends when the electron chemical potential goes to zero, at the point D . At this point, $\mu = 408$ MeV and the volume fraction of the CFL phase has reached $\chi = 1$. Beyond this density, we have homogeneous, electrically neutral, CFL matter. Fig. 6 also shows the critical point where the

pressure of electrically neutral nuclear matter equals that of \tilde{Q} -neutral CFL matter. This corresponds to the points labelled B and C , where $\mu_{BC} = 365$ MeV and $\mu_e = 214$ MeV. This corresponds to the sharp interface, discussed in §3 and §4 and shown in Fig. 3. We shall show below that this sharp interface is favored, even though it is evidently not favored by the bulk free energies, if it is stabilized by a sufficiently large surface tension. Note that in the neutral CFL matter to the right of the sharp interface, μ_e is the same as that at B while $\mu_e^{\text{eff}} = 0$ as a result of the electric field at the interface. In this way, the bulk CFL matter remains neutral (with no electrons or kaons) even in the presence of a large μ_e . In the mixed phase, by contrast, there are no significant electric fields, $\mu_e^{\text{eff}} = \mu_e$ decreases continuously, and the CFL+kaon matter is negatively charged. The kaon condensate occurs only in that region of the mixed phase where $\mu_e > m_K$. In Fig. 6, $\mu_e = m_K$ at $\mu = 398$ MeV. Between this point and D , the negatively charged CFL component of the mixed phase contains electrons but no kaons.

We must now evaluate the surface and Coulomb energy costs associated with the mixed phase, in order to make a fair comparison between it and the sharp interface. We have seen in §5 that the surface tension between a region of CFL matter and a region of nuclear matter is very large if the regions themselves extend over distances much greater than the electron Debye length $\lambda_e \sim 10$ fm. From this we conclude that a mixed phase is only possible if the size of the CFL and nuclear regions within the mixed phase are comparable to or smaller than λ_e . If this condition is satisfied, the particle number densities will be reasonably constant across a single CFL region or across a single nuclear region. (See Refs. [36, 37, 38] for demonstrations, in different contexts, that the relevant length scale is within a factor of two of λ_e .) In a sense, if the characteristic length scale r_0 of the domains within the mixed phase is smaller than λ_e , the mixed phase region is “all boundary layer”. If $r_0 < \lambda_e$ the surface tension whose free energetic cost we must yet take into account is dominated by σ_{QCD} , that of the QCD-scale micro-boundaries between CFL and nuclear domains. If $r_0 < \lambda_e$ we may neglect corrections due to the (small) variation of particle densities within regions of size r_0 .

For what value of σ_{QCD} is the mixed phase energetically favored? To answer this, we will treat σ_{QCD} as an independent parameter, constant across the whole mixed phase. In fact, σ_{QCD} depends on both μ and μ_e ,⁵ but in our simple parametric study we will ignore this dependence and adopt the method outlined in Ref. [35] to estimate the surface and Coulomb energy cost of the mixed phase. The mixed phase can be subdivided into electrically neutral unit cells called Wigner-Seitz cells, as in the analysis of the inner crust of a neutron star where droplets of charged nuclear matter coexist with a negatively charged fluid of neutrons and electrons [39]. In the present context, each Wigner-Seitz cell will contain some positively charged nuclear matter

⁵The difference between the energy densities of the two phases found at a given location within the mixed phase varies between about 300 and 350 MeV/fm³ as the mixed phase is traversed. As for the single sharp interface, therefore, naive dimensional analysis suggests a microboundary surface tension $\sigma_{\text{QCD}} \sim 300$ MeV/fm².

and some negatively charged CFL+kaon matter. Although at low temperature these unit cells form a Coulomb lattice, the interaction between adjacent cells can be neglected compared to the surface and Coulomb energy of each cell. In this Wigner-Seitz approximation, the surface and Coulomb energy per unit volume are fairly straightforward to calculate. They depend in general on the geometry and are given by [40]

$$E^S = \frac{d x \sigma_{\text{QCD}}}{r_0}, \quad (6.3)$$

$$E^C = 2\pi \alpha_{\text{em}} f_d(x) (\Delta Q)^2 r_0^2, \quad (6.4)$$

where d is the dimensionality of the structure ($d = 1, 2$, and 3 correspond to Wigner-Seitz cells describing slab, rod and droplet configurations, respectively), σ is the surface tension and $\Delta Q = Q_{\text{nuclear}} - Q_{\text{CFL+kaons}}$ is the charge density contrast between the two phases. The other factors appearing in Eqs. (6.3),(6.4) are: x , the fraction of the rarer phase which is equal to χ where $\chi \leq 0.5$ and $(1 - \chi)$ where $0.5 \leq \chi \leq 1$; r_0 , the radius of the rarer phase (radius of drops or rods and half-thickness of slabs); and $f_d(x)$, the geometrical factor that arises in the calculation of the Coulomb energy which can be written as

$$f_d(x) = \frac{1}{d+2} \left(\frac{2-d x^{1-2/d}}{d-2} + x \right). \quad (6.5)$$

The first step in the calculation is to evaluate r_0 by minimizing the sum of E^C and E^S . The result is

$$r_0 = \left[\frac{d x \sigma_{\text{QCD}}}{4\pi \alpha_{\text{em}} f_d(x) (\Delta Q)^2} \right]^{1/3}. \quad (6.6)$$

We then use this value of r_0 in Eqs. (6.3),(6.4) to evaluate the surface and Coulomb energy cost per unit volume

$$E^S + E^C = \frac{3}{2} (4\pi \alpha_{\text{em}} d^2 f_d(x) x^2)^{1/3} (\Delta Q)^{2/3} \sigma_{\text{QCD}}^{2/3}. \quad (6.7)$$

We must now compare this cost to the bulk free energy benefit of the mixed phase.

The lowest curve in Fig. 7 shows $\Delta\Omega$, the difference between the free energy density of the mixed phase (calculated without including the surface and Coulomb energy cost) and the homogeneous electrically neutral nuclear and CFL phases separated by a single sharp interface. For $\mu \leq 365$ MeV, $\Delta\Omega = \Omega_{\text{mixed}} - \Omega_{\text{nuclear}}$; for $\mu \geq 365$ MeV, where $\Omega_{\text{CFL}} \leq \Omega_{\text{nuclear}}$, $\Delta\Omega = \Omega_{\text{mixed}} - \Omega_{\text{CFL}}$. $\Delta\Omega$ is the difference between the $P_{\text{NM/CFL}}$ and P_{Mixed} curves between A and D in Fig. 6. The mixed phase has lower bulk free energy, so $\Delta\Omega$, plotted in Fig. 7, is negative.

The remaining curves in Fig. 7 show the sum of the bulk free energy difference $\Delta\Omega$ and $(E^S + E^C)$, the surface and Coulomb energy cost of the mixed phase calculated using Eq. (6.7) for droplets, rods and slabs for three different values of

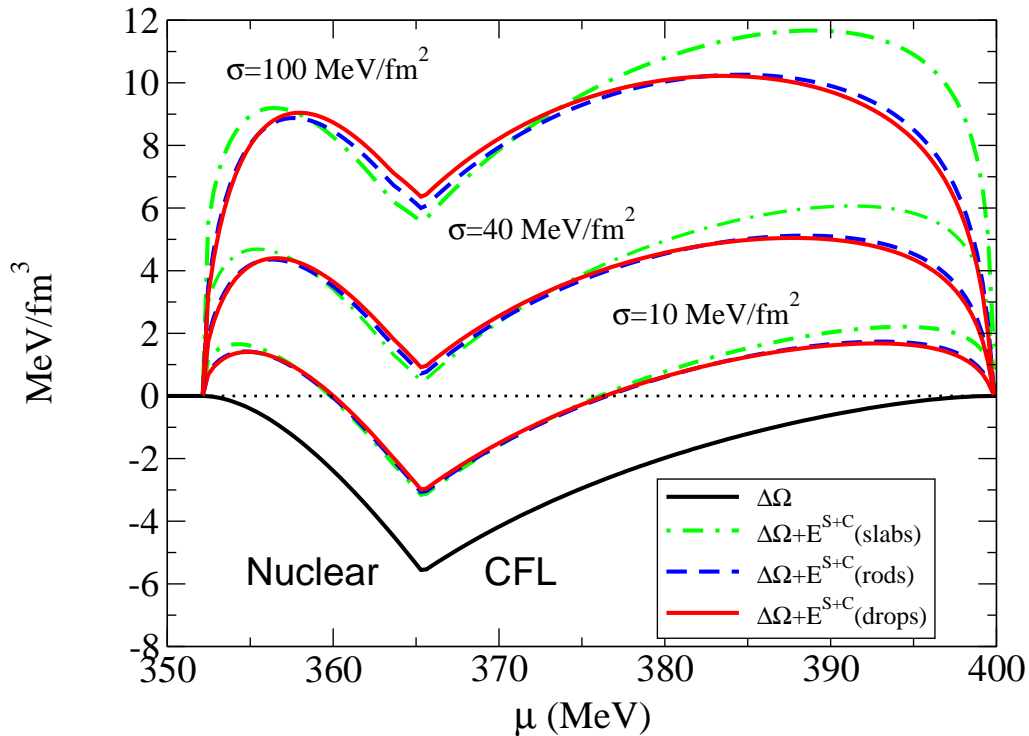


Figure 7: The free energy difference between the mixed phase and the homogeneous neutral nuclear and CFL phases. In the lowest curve, the surface and Coulomb energy costs of the mixed phase are neglected, and the mixed phase therefore has the lower free energy. Other curves include surface and Coulomb energy for different values of σ_{QCD} and different mixed phase geometry. As σ_{QCD} increases, the surface and Coulomb price paid by the mixed phase increases.

σ_{QCD} . Careful inspection of the figure reveals that for any value of σ_{QCD} , the mixed phase is described as a function of increasing density by a progression from drops to rods to slabs of CFL matter within nuclear matter to slabs to rods to drops of nuclear matter within CFL matter. This is the same progression of geometries seen in the inner crust of a neutron star [41] or in the mixed phase at a first order phase transition between nuclear matter and a hadronic kaon condensate [42] or unpaired quark matter [36]. We have also checked that for $\sigma_{\text{QCD}} = 10$ and 40 MeV/fm^2 , with the mixed phase geometry at any χ taken to be that favored, the sizes of regions of both the rarer and more common phases (r_0 and its suitably defined counterpart) are always less than $5 - 6 \text{ fm}$. As this is less than λ_e , we are justified in our neglect of any spatial variation within regions of a single phase, and are justified in our assertion that σ_{QCD} is the relevant surface tension in the calculation of E^S .

For any given σ_{QCD} , the mixed phase has lower free energy than homogeneous neutral CFL or nuclear matter wherever one of the curves in Fig. 7 for that σ_{QCD} is negative. We see that much of the mixed phase will survive if $\sigma_{\text{QCD}} \simeq 10 \text{ MeV/fm}^2$

while for $\sigma_{\text{QCD}} \gtrsim 40 \text{ MeV/fm}^2$ the mixed phase is not favored for any μ . This means that if the QCD-scale surface tension $\sigma_{\text{QCD}} \gtrsim 40 \text{ MeV/fm}^2$, the single sharp interface with its attendant boundary layers, described in previous sections, is free-energetically favored over the mixed phase.

7 Looking Ahead to Neutron Star Structure and Collisions

According to the considerations of this paper, neutron stars plausibly consist of nuclear matter of relatively low density floating on a dense CFL core, with a baryon and energy density discontinuity of about a factor of two at the astrophysically sharp interface separating them. Further work is certainly required to determine the location in μ , and ultimately in pressure and radius, of such an interface. A better understanding of the QCD-scale surface tension is required in order to confirm that the single sharp interface is stable against the formation of a broad mixed phase region. A mixed phase region would have distinctive characteristics. Its transport properties are very different from those of the uniform CFL state: neutrino mean free paths, which are long in the CFL phase [43], are very short in the mixed phase due to coherent scattering [44]. Ultimately, therefore, features in the temporal distribution of neutrinos emitted by a supernova and detected in an underground detector may allow a conclusive determination of whether a mixed phase region does or does not form. For the present, naive dimensional analysis suggests that $\sigma_{\text{QCD}} \sim 300 \text{ MeV}$, significantly greater than the minimum $\sigma_{\text{QCD}} \sim 40 \text{ MeV}$ required to ensure that the sharp interface is favored. If present, the sharp interface has interesting properties at the tens of fermi length scale: a large pileup of protons on the nuclear side of the interface and a large amplitude kaon condensate on the CFL side of the interface.

From the point of view of neutron star structure, though, the most important consequence of its presence is simply the discontinuous change in the density by about a factor of two. This will have quantitative effects on the mass vs. radius relationship for neutron stars with quark matter cores. It may also have qualitative effects on the gravitational wave profile emitted during the inspiral and merger of two compact stars of this type. One may expect characteristic features in the gravitational waves to arise both when the outer nuclear matter portions of the star begin to deform each other and then somewhat later when the denser CFL cores begin to deform. Neutron stars with two important length scales (the star radius and the core radius) will introduce features on two timescales in the gravitational waves produced late in an inspiral event.

Acknowledgements

We acknowledge helpful conversations with G. F. Bertsch, R. L. Jaffe and D. B. Kaplan. The work of MA is supported in part by UK PPARC. The work of SR is supported in part by the U.S. Department of energy (DOE) under grant #DE-FG03-00ER4132. The work of KR and FW is supported in part by the DOE

under cooperative research agreement #DF-FC02-94ER40818. The work of KR is supported in part by a DOE OJI Award and by the Alfred P. Sloan Foundation.

References

- [1] M. Alford, K. Rajagopal and F. Wilczek, Nucl. Phys. **B537**, 443 (1999) [hep-ph/9804403].
- [2] R. Rapp, T. Schäfer, E. V. Shuryak and M. Velkovsky, Annals Phys. **280**, 35 (2000) [hep-ph/9904353]; T. Schäfer, Nucl. Phys. **B575**, 269 (2000) [hep-ph/9909574]; I. A. Shovkovy and L. C. Wijewardhana, Phys. Lett. **B470**, 189 (1999) [hep-ph/9910225]; N. Evans, J. Hormuzdiar, S. D. Hsu and M. Schwetz, Nucl. Phys. **B581**, 391 (2000) [hep-ph/9910313].
- [3] For a review, see K. Rajagopal and F. Wilczek, to appear in B. L. Ioffe Festschrift, “At the Frontier of Particle Physics / Handbook of QCD”, M. Shifman, ed., (World Scientific, 2001) [hep-ph/0011333].
- [4] For a review, see M. Alford, to appear in Annu. Rev. Nucl. Part. Sci. [hep-ph/0102047].
- [5] R. Casalbuoni and R. Gatto, Phys. Lett. **B464**, 111 (1999) [hep-ph/9908227].
- [6] D. T. Son and M. A. Stephanov, Phys. Rev. **D61**, 074012 (2000) [hep-ph/9910491]; erratum, *ibid.* **D62**, 059902 (2000) [hep-ph/0004095].
- [7] D. K. Hong, T. Lee and D. Min, Phys. Lett. **B477**, 137 (2000) [hep-ph/9912531].
- [8] C. Manuel and M. H. Tytgat, Phys. Lett. **B479**, 190 (2000) [hep-ph/0001095].
- [9] M. Rho, E. Shuryak, A. Wirzba and I. Zahed, Nucl. Phys. **A676**, 273 (2000) [hep-ph/0001104].
- [10] K. Zarembo, Phys. Rev. **D62**, 054003 (2000) [hep-ph/0002123].
- [11] S. R. Beane, P. F. Bedaque and M. J. Savage, Phys. Lett. **B483**, 131 (2000) [hep-ph/0002209].
- [12] D. K. Hong, Phys. Rev. **D62**, 091501 (2000)
- [13] C. Manuel and M. H. Tytgat, Phys. Lett. B **501**, 200 (2001) [hep-ph/0010274].
- [14] R. Casalbuoni, R. Gatto and G. Nardulli, Phys. Lett. B **498**, 179 (2001) [hep-ph/0010321].

- [15] M. Alford, J. Berges and K. Rajagopal, Nucl. Phys. **B558**, 219 (1999) [hep-ph/9903502].
- [16] T. Schäfer and F. Wilczek, Phys. Rev. **D60**, 074014 (1999) [hep-ph/9903503].
- [17] K. Rajagopal and F. Wilczek, to appear in Phys. Rev. Lett., hep-ph/0012039.
- [18] M. Alford, J. Berges and K. Rajagopal, Nucl. Phys. **B571**, 269 (2000) [hep-ph/9910254].
- [19] C. Alcock, E. Farhi and A. Olinto, Astrophys. J. **310**, 261 (1986).
- [20] N. K. Glendenning, Phys. Rev. D **46**, 1274 (1992).
- [21] D. B. Kaplan and A. E. Nelson, Phys. Lett. B **175**, 57 (1986).
- [22] T. Schäfer and F. Wilczek, Phys. Rev. Lett. **82**, 3956 (1999) [hep-ph/9811473].
- [23] A. I. Larkin and Yu. N. Ovchinnikov, Zh. Eksp. Teor. Fiz. **47**, 1136 (1964) [Sov. Phys. JETP **20**, 762 (1965)]; P. Fulde and R. A. Ferrell, Phys. Rev. **135**, A550 (1964).
- [24] M. Alford, J. Bowers and K. Rajagopal, Phys. Rev. D **63**, 074016 (2001) [hep-ph/0008208].
- [25] J. Bowers, J. Kundu, K. Rajagopal, E. Shuster, to appear in Phys. Rev. D. [hep-ph/0101067].
- [26] A. Leibovich, K. Rajagopal and E. Shuster, hep-ph/0104073.
- [27] B. A. Freedman and L. D. McLerran, Phys. Rev. **D16**, 1169 (1977).
- [28] E. Farhi and R. L. Jaffe, Phys. Rev. D **30**, 2379 (1984), and references therein.
- [29] T. Schäfer, Phys. Rev. **D62**, 094007 (2000) [hep-ph/0006034].
- [30] N. K. Glendenning, *Compact Stars, Nuclear Physics, Particle Physics and General Relativity*, (Springer-Verlag, New York, 1997)
- [31] B. Serot and J. D. Walecka, *Advances in Nucl. Physics*, **16**, edited by J. W. Negele and E. Vogt (Plenum, New York, 1986)
- [32] D. H. Rischke, D. T. Son and M. A. Stephanov, hep-ph/0011379.
- [33] T. Schäfer, Phys. Rev. Lett. **85**, 5531 (2000) [nucl-th/0007021].
- [34] M. Prakash, J. R. Cooke and J. M. Lattimer, Phys. Rev. D **52**, 661 (1995).
- [35] N. K. Glendenning and S. Pei, Phys. Rev. C **52**, 2250 (1995).

- [36] H. Heiselberg, C. J. Pethick and E. F. Staubo, Phys. Rev. Lett. **70**, 1355 (1993).
- [37] H. Heiselberg, Phys. Rev. D **48**, 1418 (1993).
- [38] T. Norsen and S. Reddy, nucl-th/0010075.
- [39] G. Baym, H. A. Bethe, C. J. Pethick, Nucl. Phys. A175, 225 (1971); J. Negele and D. Vautherin, Nucl Phys **A207**, 298 (1973).
- [40] D. G. Ravenhall, C. J. Pethick, J. R. Wilson, Phys. Rev. Lett. **50**, 2066 (1983).
- [41] D. G. Ravenhall, C. J. Pethick and J. R. Wilson, Phys. Rev. Lett. **50**, 2066 (1983); D. G. Ravenhall and C. J. Pethick, Annu. Rev. Nucl. Part. Sci. **45**, 429, (1995).
- [42] N. K. Glendenning and J. Schaffner-Bielich, Phys. Rev. Lett. **81**, 4564 (1998).
- [43] G. W. Carter and S. Reddy, Phys. Rev. D **62**, 103002 (2000) [hep-ph/0005228].
- [44] S. Reddy, G. Bertsch and M. Prakash, Phys. Lett. B **475**, 1 (2000) [nucl-th/9909040].